ELSEVIER

Contents lists available at ScienceDirect

# **BBA** - Biomembranes

journal homepage: www.elsevier.com/locate/bbamem





# Pinholin $S^{21}$ mutations induce structural topology and conformational changes

Tanbir Ahammad <sup>a</sup>, Rasal H. Khan <sup>a</sup>, Indra D. Sahu <sup>a,b</sup>, Daniel L. Drew Jr. <sup>a</sup>, Emily Faul <sup>a</sup>, Tianyan Li <sup>a</sup>, Robert M. McCarrick <sup>a</sup>, Gary A. Lorigan <sup>a,\*</sup>

#### ARTICLE INFO

Keywords:
Holin
Pinholin
DEER spectroscopy
CW-EPR power saturation
Mutational effect

#### ABSTRACT

The bacteriophage infection cycle is terminated at a predefined time to release the progeny virions via a robust lytic system composed of holin, endolysin, and spanin proteins. Holin is the timekeeper of this process. Pinholin  $S^{21}$  is a prototype holin of phage  $\Phi 21$ , which determines the timing of host cell lysis through the coordinated efforts of pinholin and antipinholin. However, mutations in pinholin and antipinholin play a significant role in modulating the timing of lysis depending on adverse or favorable growth conditions. Earlier studies have shown that single point mutations of pinholin  $S^{21}$  alter the cell lysis timing, a proxy for pinholin function as lysis is also dependent on other lytic proteins. In this study, continuous wave electron paramagnetic resonance (CW-EPR) power saturation and double electron-electron resonance (DEER) spectroscopic techniques were used to directly probe the effects of mutations on the structure and conformational changes of pinholin S21 that correlate with pinholin function. DEER and CW-EPR power saturation data clearly demonstrate that increased hydrophilicity induced by residue mutations accelerate the externalization of antipinholin transmembrane domain 1 (TMD1), while increased hydrophobicity prevents the externalization of TMD1. This altered hydrophobicity is potentially accelerating or delaying the activation of pinholin S21. It was also found that mutations can influence intra- or intermolecular interactions in this system, which contribute to the activation of pinholin and modulate the cell lysis timing. This could be a novel approach to analyze the mutational effects on other holin systems, as well as any other membrane protein in which mutation directly leads to structural and conformational changes.

#### 1. Introduction

Bacteriophages are the most abundant organism in the biosphere, recycling much of the world's biomass through  $\sim 10^{28}$  infection cycles per day [1,2]. Phages have evolved a robust lytic system to control the length of the infection cycle so that it can be adjusted for different environments and host populations [3,4]. Most large, dsDNA bacteriophages use at least three different proteins (holin, endolysin, and spanin) to lyse gram-negative bacteria by permeabilizing and degrading the cytoplasmic membrane, peptidoglycan layer, and cell wall, respectively [5–9]. The holin protein functions as an allele-specific molecular timer that triggers the formation of microscale holes for the release of fully-folded functional endolysin [4,5,10–21]. Although the holin-endolysin system is a robust and efficient lytic system,  $\sim 25\%$  of phages employ a prototype evolutionarily intermediate lytic system, known as the pinholin-SAR (signal anchor release) endolysin system, which is

underrepresented in the literature [22]. Pinholins make nanoscale holes which are not large enough to accommodate folded endolysin, but do allow the passage of protons to dissipate the proton motive force (PMF) which in turn leads to the release and activation of the membrane-tethered SAR-endolysin for its muralytic action [10,22].

Pinholin  $S^{21}$  from lambdoid phage  $\Phi 21$  is one of the most well-studied pinholin systems [10,23–30]. This system features two pinholin proteins, an active pinholin ( $S^{21}68$ ) and an antipinholin ( $S^{21}71$ ). Both pinholin proteins have two transmembrane domains (TMDs) and accumulate benignly in the cytoplasmic membrane as an inactive dimer where both TMDs reside in the bilayer. For pinhole formation, TMD1 of  $S^{21}$  must be externalized from the lipid bilayer. For  $S^{21}68$ , TMD1 externalization is a rapid and spontaneous process (Fig. 1). The externalization of  $S^{21}71$  TMD1 is much slower relative to  $S^{21}68$  due to the presence of an additional positively charged Lys residue in the N-terminal region. The presence of  $S^{21}71$  delays the pinhole formation

E-mail address: gary.lorigan@miamioh.edu (G.A. Lorigan).

<sup>&</sup>lt;sup>a</sup> Department of Chemistry and Biochemistry, Miami University, Oxford, OH 45056, USA

<sup>&</sup>lt;sup>b</sup> Natural Science Division, Campbellsville University, Campbellsville, KY 42718, USA

<sup>\*</sup> Corresponding author.

[10,24]. S<sup>21</sup>71 is a weak antipinholin as it can only delay but not completely block the externalization of TMD1 [24]. The Ry Young lab has reported the generation of a more dominant antipinholin by inserting five amino acids (RYIRS) into the N-terminal region of S<sup>21</sup>68. The externalization of TMD1 is blocked because of the addition of more positive charges and bulky side chains (Fig. 1) [24]. This antipinholin variant is denoted by S<sup>21</sup>68<sub>IRS</sub> [24]. In this study, S<sup>21</sup>68<sub>IRS</sub> replaced S<sup>21</sup>71 in the pinholin system to determine the mutation effect on inactive antipinholin.

Phages use a combination of holin and antiholin to adjust the timing of lysis [3,22]. In addition, phages tune their lytic function by the mutation of endolysin and/or holin to adjust to various hosts and environments [3,22]. In the case of phage  $\Phi$ 21, the mutation of SARendolysin alone is not a viable strategy for the phage to adjust the lysis timing since there are very few mutation options within the membrane-tethered N-terminal region of SAR-endolysin that do not alter its effective turnover number (Kcat) [22]. Hence, mutation of pinholin could be the mechanism by which phage  $\Phi$ 21 adjusts lysis timing for changing environments. Pang et al. (2010) reported an extensive mutational study of S<sup>21</sup> with a wide range of phenotypes, including absolute lysis defective variants, as well as those with delayed or accelerated lysis triggering [24]. Although S<sup>21</sup>68<sub>IRS</sub> has been shown to be the dominant antipinholin that prevents cell lysis, some mutations rendered it active and abolished its antiholin properties [24]. In that study, more emphasis was given to S<sup>21</sup>68, and fewer mutants of S<sup>21</sup>68<sub>IRS</sub> were examined. Cell lysis time was monitored to determine the mutational effects, although this is not enough to define pinholin activity as SAR endolysin alone can cause lysis after induction, regardless of expression of the pinholin allele [22,24].

This study reports the effects of various mutations on the structural and topological properties of antipinholin  $\mathrm{S}^{21}68_{\mathrm{IRS}}$  using CW-EPR power saturation and DEER spectroscopic techniques. To examine the mutational effect on the structural topology, we studied eight single spinlabeled and seven double spin-labeled mutants with or without further substitution of wild-type amino acids. This work directly evaluated the structural and conformational changes of  $\mathrm{S}^{21}68_{\mathrm{IRS}}$  and correlated those observed with activation or inactivation of the protein from a previous

biological study [24]. This mutational study clearly demonstrates that the relative hydrophobicity of TMD1 impacts its externalization, which further controls the activation and pinhole formation. In addition, mutations also changed how TMD1 and TMD2 interact, which ultimately impacted the externalization of TMD1, leading to alteration of triggering time. These results provide a much more comprehensive picture of the mutational effects on the structural topology and conformational changes of  $\rm S^{21}68_{IRS}$  and explain how these conformational changes influence the functionality of the pinholin system.

### 2. Experimental methods

#### 2.1. Peptide synthesis, spin labeling, and purification

Seventy-three amino acid long S<sup>21</sup>68<sub>IRS</sub> (Fig. 1) peptides were synthesized on an automated CEM Liberty Blue peptide synthesizer equipped with the Discovery Bio microwave system, via optimized Fmoc solid-phase peptide synthesis (SPPS), as reported in previous studies [25,26]. In brief, each synthesis was started with 0.1 mM glutamate preloaded TGA resin. The synthesis was performed in the dimethylformamide (DMF) based solvent system. Piperidine (20% v/v), N,N'diisopropylcarbodiimide (DIC) (15.6% v/v), and oxyma (14.2% w/v) in DMF were used as a deprotecting agent, activator, and activator base, respectively. During each coupling cycle, 0.2 M amino acid was added to the reaction vessel in the presence of activator and activator base. After successful synthesis, the crude peptide was obtained following a previously published optimized cleavage procedure [25,26,31,32]. The crude peptide was purified by reverse-phase high-performance liquid chromatography (RP-HPLC) using a GE HPLC system coupled with a C4 (10  $\mu m$ ) preparative column (Vydac 214TP, 250  $\times$  22 mm), following the optimized method [25,26].

To attach the spin label (SL) to the peptides, eight single Cys and seven double Cys mutants were synthesized with or without further substitution of wild type amino acids. The lyophilized pure peptides with Cys in designated location(s) were dissolved in dimethyl sulfoxide (DMSO) with a 5-fold excess of MTSL (S-(1-oxyl-2,2,5,5-tetramethyl-2,5-dihydro-1H-pyrrol-3-yl) methyl ethanesulfonothioate) per Cys

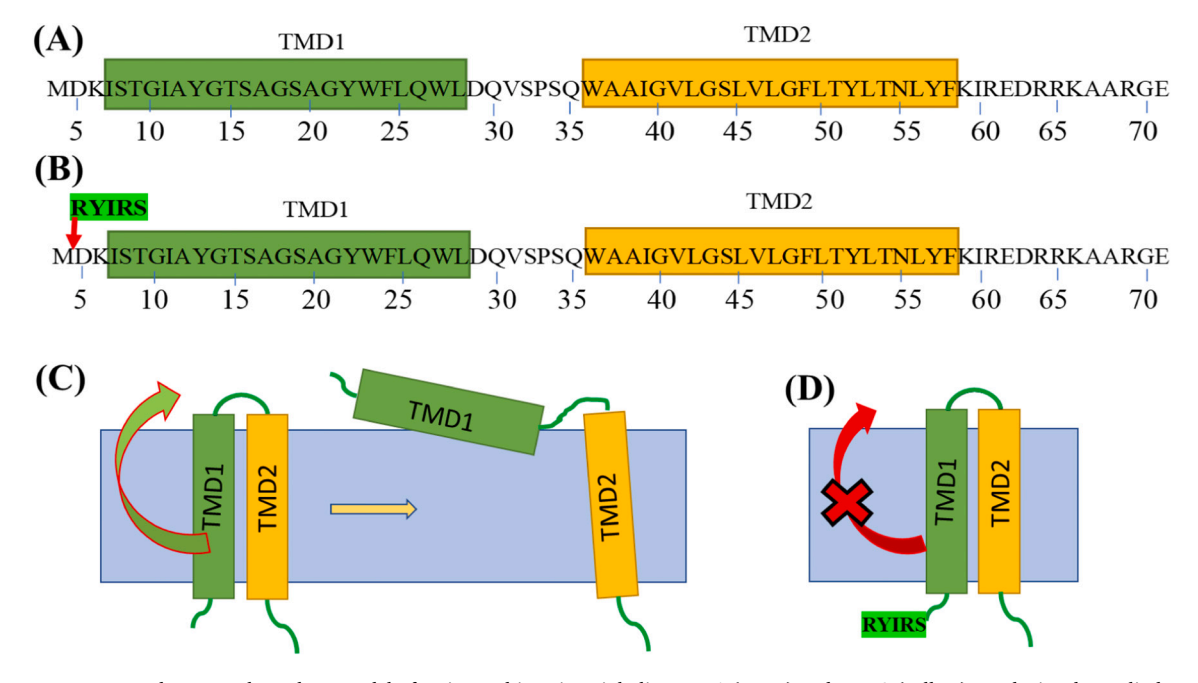


Fig. 1. Primary sequence and structural topology model of active and inactive pinholin. TMD1 (green) and TMD2 (yellow) are depicted as cylinders. (A) and (B) show the primary amino acid sequences of  $S^{21}68$  and  $S^{21}68_{IRS}$  where an 'RYIRS' tag has been incorporated between Met4 and Asp5 in the N-terminus of  $S^{21}68_{IRS}$ . (C) and (D) show the possible topology models of  $S^{21}68$  and  $S^{21}68_{IRS}$ , respectively [25,29,30]. (For interpretation of the references to color in this figure legend, the reader is referred to the web version of this article.)

residue (1:5 M ratio for the single spin label and 1:10 M ratio for the dual spin label) and stirred for 24 h in the dark at room temperature. The spin labeled peptide was further purified using a C4 semi-preparative column (Vydac 214TP,  $250 \times 10$  mm) to remove unbound MTSL and other contaminants [25,26]. After each purification, the purity and identity of the target peptide were confirmed by MALDI-TOF MS. Spin labeling efficiency was  $\sim$ 85–90% as calculated by CW-EPR measurements [26].

#### 2.2. Peptide incorporation into proteoliposomes

To mimic the membrane environment, spin labeled antipinholin peptides were incorporated into DMPC (1,2-Dimyristoyl-sn-Glycero-3-Phosphocholine) proteoliposomes using the thin film method [25,26]. DMPC lipid was used as a standard model lipid and optimized for the incorporation of pinholin S<sup>21</sup> peptide in our earlier spectroscopic studies [26,27]. In brief, the peptide was dissolved in 2,2,2-Trifluoroethanol and mixed with DMPC solution in a pear-shaped flask. The organic solvents were gently evaporated by nitrogen gas purging with the continuous rotation of flask to form a uniform thin film. To prepare the samples for CW-EPR and power saturation experiments, a 10 mM HEPES (4-(2-hydroxyethyl)-1-piperazineethanesulfonic acid) buffer (pH 7.0) was used to rehydrate the thin film. The peptide: lipid ratio was 1:1000 in the final proteoliposomes sample. Glycerol was added to a final concentration of 10% to help the sample remain suspended for a longer duration at room temperature without phase separation [25]. For DEER samples, 20 mM HEPES (4-(2-hydroxyethyl)-1-piperazineethanesulfonic acid) buffer in  $D_2O$  (pH ~7.0) was used to rehydrate the thin film [29]. The final peptide concentration was 50 µM for DEER samples with 1:1000 ratio of peptide:lipid [29]. This ratio was chosen to minimize the effect of intermolecular interactions between monomers of pinholin which have been shown to oligomerize in the penultimate step of the lysis mechanism [23,28]. Glycerol was added to each DEER samples at a 30% (v/v) final concentration as a cryoprotectant. Before rehydration of any proteoliposome sample, both HEPES buffer and the sample flask were kept in a warm water bath for a short period of time to bring the temperature above the phase transition temperature of DMPC [25,29,33,34]. Dynamic light scattering (DLS) spectroscopy (ZETA-SIZER NANO Series; Malvern Instruments) was used to confirm the size and homogeneity of the proteoliposomes in each sample; the average size (diameter) of the proteoliposomes was  $\sim$ 200 nm [25].

#### 2.3. CW-EPR spectroscopy

All EPR experiments were conducted at the Ohio Advanced EPR Laboratory at Miami University. CW-EPR spectra were collected at X-band (~9.34 GHz) with a Bruker EMX spectrometer equipped with ER041xG microwave bridge and ER4119-HS cavity. Each spectrum was acquired by signal averaging 10 scans with 3315 G central field, 150 G sweep width, 42 s field sweep, 100 kHz modulation frequency, 1 G modulation amplitude, and 10 mW microwave power [25].

#### 2.4. CW-EPR power saturation experiments

CW-EPR power saturation experiments were performed on a Bruker EMX X-band spectrometer coupled with ER 041XG microwave bridge and ER 4123D CW-resonator (Bruker BioSpin). Experimental setups were optimized following previously published literature [35–37]. 3–4  $\mu L$  samples were loaded into a gas permeable TPX capillary tube at a concentration of 100–150  $\mu M$  [35,38–40]. EPR spectroscopic data was collected using a modulation amplitude of 1.0 G, a modulation frequency of 100 kHz, 42 s field sweep, and 90 G sweep width [25]. Incident microwave power was varied from 0.05 mW to 126 mW. For each spin labeled site, the spectra were recorded under three equilibrium conditions; oxygen, nitrogen, and NiEDDA equilibriums, as described in previous literature [25,40]. CW-EPR power saturation data were extracted and analyzed using a MATLAB software script. The peak-to-

peak amplitudes of the first derivative central resonance lines (A) were extracted and plotted against the square root of the incident microwave power (P). These data points were then fitted according to Eq. (1): [39,41]

$$A = I\sqrt{P} \left[ 1 + \frac{\left(2^{\frac{1}{\varepsilon}} - 1\right)P}{P_{\frac{1}{2}}} \right]^{-\varepsilon} \tag{1}$$

where I is the scaling factor,  $\varepsilon$  is the homogeneity of saturation of the resonance line, and  $P_{1/2}$  is the power where the first derivative amplitude is reduced to half of its unsaturated value.  $\varepsilon$  values varied between 1.5 and 0.5 for the homogeneous to inhomogeneous saturation, respectively [41]. In Eq. (1), I,  $\varepsilon$ , and  $P_{1/2}$  are adjustable parameters and yield a characteristic  $P_{1/2}$  value for each equilibrium condition. The corresponding depth parameter ( $\Phi$ ) was calculated using Eq. (2): [41]

$$\Phi = ln \left[ \frac{\Delta P_{\underline{1}}(O_2)}{\Delta P_{\underline{1}}(\text{NiEDDA})} \right]$$
 (2)

where  $\Delta P_{1/2}(NiEDDA)$  is the difference in the  $P_{1/2}$  values for NiEDDA and nitrogen equilibriums, and  $\Delta P_{1/2}(O_2)$  is the difference in the  $P_{1/2}$  values for oxygen and nitrogen equilibriums.

#### 2.5. DEER spectroscopic measurements

The four-pulse DEER experiments were conducted using a Bruker ELEXSYS E580 spectrometer with a SUPERQ-FT pulse Q-band system. For initial data collection, the system used a 10 W amplifier, however it was upgraded to a more powerful 300 W amplifier with an EN5107D2 resonator. Approximately 70  $\mu L$  of the sample was loaded into a 3 mm quartz EPR tube and flash-frozen with liquid nitrogen prior to insertion in the resonator cavity. Experimental data was collected with 16-step phase cycling at a temperature of 80 K. An optimized four-pulsed sequence  $[(\pi/2)_{\nu 1} - \tau_1 - (\pi)_{\nu 1} - t - (\pi)_{\nu 2} - (\tau_1 + \tau_2 - t) - (\pi)_{\nu 1} \tau_2$  - echo] was used for dead time free DEER experimental data collection [42,43]. The probe pulse  $(\pi)_{\nu 1}$  width was 16 ns, and pump pulse  $(\pi)_{1/2}$  width was 24 ns. 120 MHz of frequency difference was used between the pump and probe pulses. In the upgraded instrumental setup, the pump pulse was a 70 ns frequency-swept chirp pulse spanning 85 MHz. The shot repetition time was 1000 µs with 100 shots/point. Data acquisition time was 2-3 µs depending on the samples' phase memory time (T2) and S/N ratio. Data acquisition was done overnight for signal averaging. The DEER data analysis was conducted using the MATLAB DEER Analysis 2015 Program [44,45]. DEER distance distributions, P(r), were obtained using Tikhonov regularization in the distance domain with a minimum distance constraint P(r) > 0 under DEER Analysis 2015 [45]. The background correction was performed using a two-dimensional homogeneous model for proteoliposomes. The best fit of the time domain data was used for optimizing the regularization parameter in the L-curve.

#### 3. Results and discussion

Recently, we reported the structural dynamics and topology of active pinholin (S $^{21}68$ ) and inactive antipinholin (S $^{21}68_{IRS}$ ) incorporated into DMPC proteoliposomes using CW-EPR line-shape analysis, power saturation, and DEER spectroscopic experiments [25,29,30]. Fig. 1 shows the primary sequence of S $^{21}68$  and S $^{21}68_{IRS}$  with their structural topology model adapted from the literature [10,25,30].

For EPR spectroscopic experiments, a nitroxide spin label was attached to the pinholin peptide using site directed spin labeling (SDSL) [46,47]. In our previous structural studies of  $S^{21}$ , the spin label positions were judiciously selected to preserve the native conformations of active and inactive pinholin and consciously omitted those sites which might induce structural or functional perturbations according to the literature [24,25,30]. The structural perturbations induced by the spin labels were

more prominent for the inactive antipinholin since its TMD1 has a natural tendency for externalization from the lipid bilayer. It was hypothesized that those specific residue positions have a significant mutational effect. Taking into account these observations and the previous mutational study reported by Pang et al. (2010), certain residue positions (e.g. G14, S16, A17) were selected to study the mutational

effects on the structure and topology of  $S^{21}68_{IRS}$  [24].

3.1. Probing the mutational effect on the pinholin conformational changes using depth parameter

In this study, CW-EPR power saturation experiments were conducted

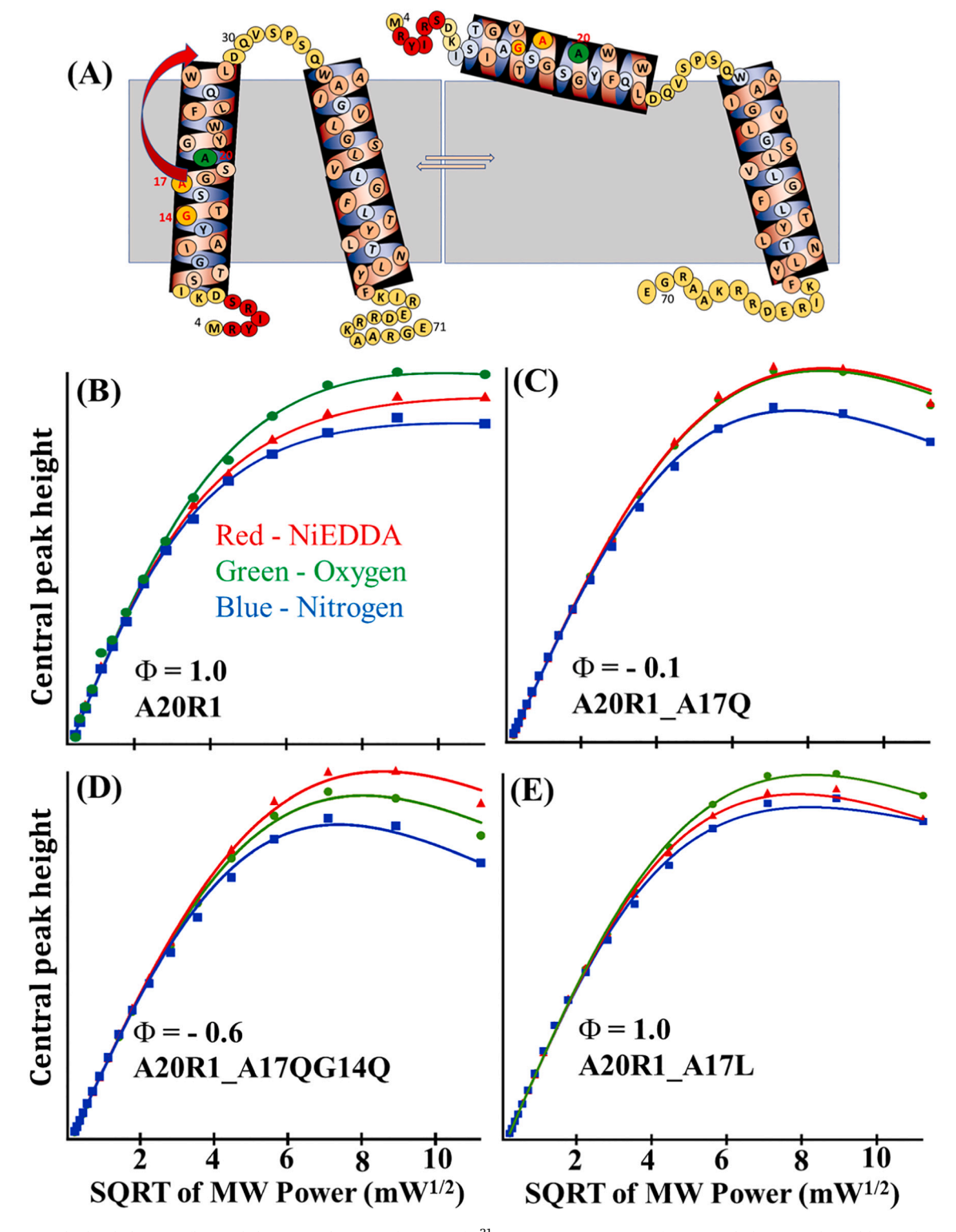


Fig. 2. Changes in hydrophobicity influenced the externalization of TMD1 of  $S^{21}68_{IRS}$ . (A) Tentative conformational change and equilibrium between two conformations of pinholin  $S^{21}$ . The position of the spin label is in green, and the points of mutation are the red letters in orange balls. CW-EPR power saturation data for IRS\_A20R1 (B), IRS\_A20R1\_A17Q (C), IRS\_A20R1\_G14QA17Q (D), and IRS\_A20R1\_A17L (E). Respective depth parameters are shown with the uncertainty of  $\pm 5\%$ . (For interpretation of the references to color in this figure legend, the reader is referred to the web version of this article.)

to investigate the mutational effect on the structural conformation of  $S^{21}68_{IRS}$  TMD1. A nitroxide spin label was placed at A20 of  $S^{21}68_{IRS}$  and denoted by IRS\_A20R1 (R1 represents the MTSL spin label attached to a Cys residue through a disulfide bond). This spin label position was selected as a control and anchoring point for the rest of the experiments since A20 is positioned approximately at the center of TMD1 and a majority of the population of A20R1 was found buried inside of the lipid bilayer (positive  $\Phi$  value) for the inactive conformation and outside of the lipid bilayer (negative  $\Phi$  value) for the active conformation, as reported previously (Fig. 1C and D) [25,30]. The  $\Phi$  values represent the relative accessibility of oxygen and NiEDDA for the nitroxide spin label and imply the relative population of the TMD1 inside vs outside of the lipid bilayer. Hence, the  $\Phi$  values obtained for IRS A20R1 in this study will report on the relative population of TMD1 inside vs outside of the lipid bilayer, which could be correlated with the inactive and active conformation of pinholin  $S^{21}$ .

Previous studies have suggested that the changes in hydrophobicity play a crucial role in the activation of pinholin by changing the probability of externalization of TMD1 [24]. To examine this effect on the conformation of  $S^{21}68_{IRS}$ , two more  $S^{21}68_{IRS}$  constructs were designed, while keeping the spin label at the A20 position, with a single mutation (A17Q), and a double mutation (G14Q and A17Q). These constructs

were denoted as IRS\_A20R1\_A17Q, and IRS\_A20R1\_G14QA17Q, respectively (Fig. 2).

The  $\Phi$  value was calculated as 1.0 for IRS\_A20R1 without an additional mutation which implied that a majority of the S<sup>21</sup>68<sub>IRS</sub> TMD1 population was located inside of the lipid bilayer. However,  $\Phi$  values of −0.1 for IRS A20R1 A17O and −0.6 for IRS A20R1 G14QA17O were measured. A more negative  $\Phi$  value indicated that a higher population of TMD1 was externalized as the hydrophilicity of the TMD1 region was increased. To examine the opposite effect, A17 was substituted with a more hydrophobic leucine (L) side chain, while keeping the spin label at the same A20R1 position of S2168<sub>IRS</sub>. The construct was denoted as IRS\_A20R1\_A17L (Fig. 2E). The  $\Phi$  value for IRS\_A20R1\_A17L was 1.0, which implied that a dominant population of S<sup>21</sup>68<sub>IRS</sub> TMD1 was inside of the lipid bilayer, similar to the inactive conformation of  $S^{21}68_{IRS}$ . This observation further confirmed that the increased hydrophobicity of TMD1 prevented the externalization of S<sup>21</sup>68<sub>IRS</sub> TMD1, while increased hydrophilicity is more likely to induce the dissociation of TMD1 from the membrane. The cumulative change of  $\Phi$  values due to changes in hydrophilicity, as observed in IRS A20R1 A17O and IRS A20R1 G14-OA170, indicated a change in the relative population of TMD1, inside vs outside of lipid bilayer. This implies a dynamic equilibrium between active and inactive conformations of pinholin S<sup>21</sup>. The increased

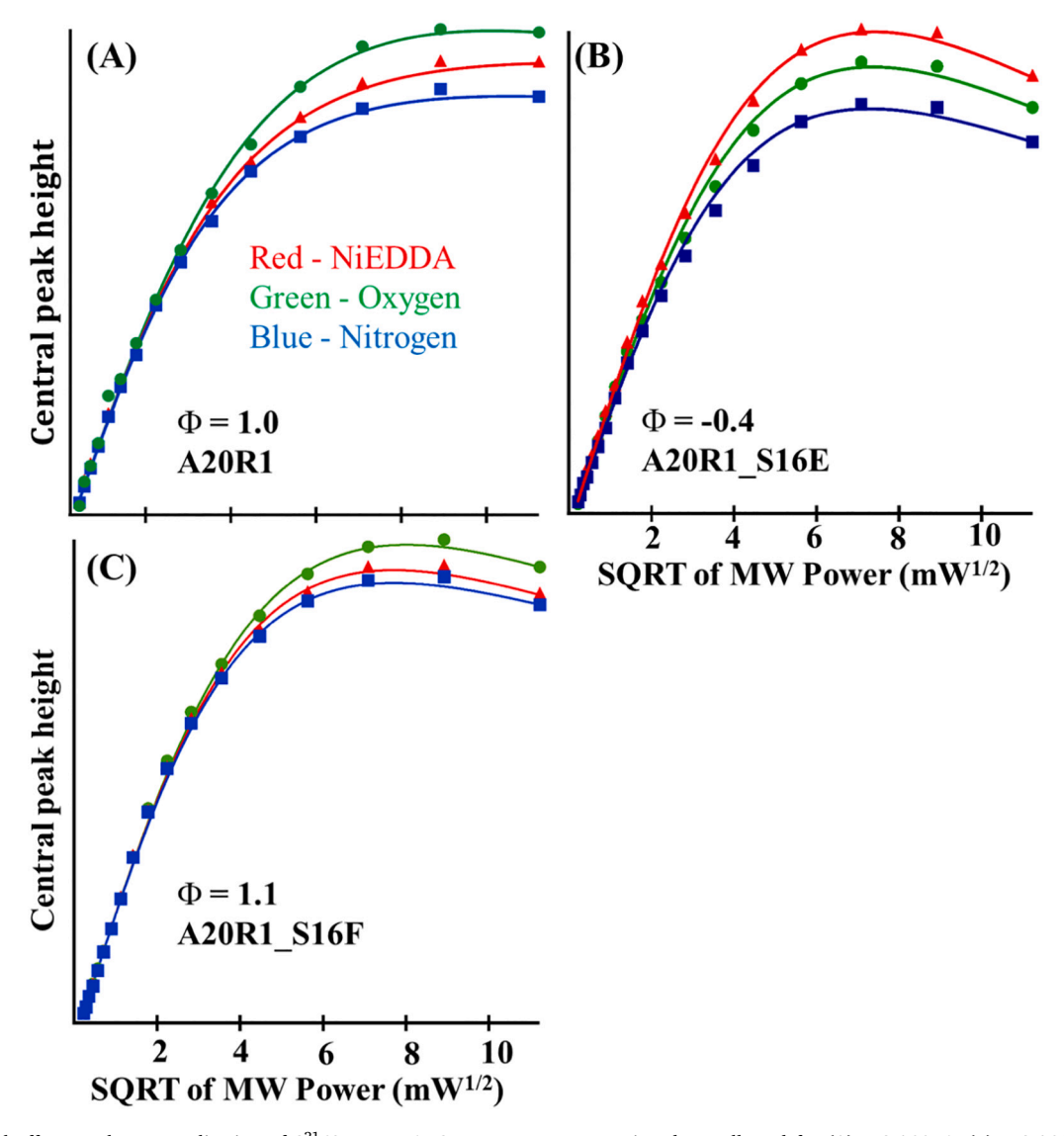


Fig. 3. Mutational effect on the externalization of  $S^{21}68_{IRS}$  TMD1. CW-EPR power saturation data collected for (A) IRS\_A20R1, (B) IRS\_A20R1\_S16E, and (C) IRS\_A20R1\_S16F. Respective depth parameters are shown with the uncertainty of  $\pm 5\%$ .

hydrophobicity of TMD1 shifted the equilibrium towards the inactive conformation and a greater population of  $S^{21}68_{IRS}$  TMD1 stayed inside of the lipid bilayer, while increased hydrophilicity shifted the equilibrium towards the active and a greater population of  $S^{21}68_{IRS}$  TMD1 was located outside of the lipid bilayer.

To further explore the effect of varying types of sidechains and charge with its hydrophobic effect, S16 was replaced with the relatively hydrophilic amino acid, glutamate (E) or relatively hydrophobic amino acid, phenylalanine (F). For direct comparison, the spin label was placed at the same A20 position. To explore the effect of these mutations on the externalization of TMD1, two constructs (IRS\_A20R1\_S16E and IRS\_A20R1\_S16F) were probed using CW-EPR power saturation experiments where the depth parameters were compared with IRS A20R1 (Fig. 3).

The  $\Phi$  value of -0.4 for IRS A20R1 S16E clearly demonstrated that a greater population of A20R1 spin-labeled TMD1 stayed outside of the lipid bilayer when compared to that for IRS A20R1 (negative vs positive  $\Phi$  value). These data implied that this mutation (S16E) enhanced the externalization of S<sup>21</sup>68<sub>IRS</sub> TMD1 and hence most of the population adapted an active conformation of pinholin S<sup>21</sup>. However, for IRS A20R1 S16F, Φ value (1.1) was similar to IRS A20R1 indicating that most of the population of A20R1 spin-labeled TMD1 was buried inside of the lipid bilayer similar to that of IRS\_A20R1 and implied that this mutation does not enhance the externalization of S<sup>21</sup>68<sub>IRS</sub> TMD1, while the majority of the population adapted an inactive conformation of pinholin S<sup>21</sup>68<sub>IRS</sub>. These observations are consistent with earlier CW-EPR power saturation data (Fig. 2) suggesting that the increased hydrophobicity of the IRS\_A20R1\_S16F variant prevented the externalization of TMD1, while increased hydrophilicity in IRS A20R1 S16E enhanced the externalization of TMD1. However, sidechain type (aromatic vs aliphatic) and charge (positively vs negatively charged) did not play a significant role on the externalization of TMD1 as observed for relative hydrophobicity of TMD1.

In addition to the mutational effect induced by the substitution of native amino acids with other amino acids, incorporation of the spin label in certain residue positions can lead to structural perturbations which are comparable to the mutational effects that caused the externalization of TMD1 of inactive pinholin. For example, for positions IRS\_S16R1 and IRS\_A17R1, it was expected that a majority of the population would be located inside of the lipid bilayer as suggested by a previous study that showed G14, S19, and A20 were located inside of the lipid bilayer for antipinholin [30]. However, the calculated depth parameters  $(\Phi)$  were -0.8 and -1.0 for IRS S16R1 and IRS A17R1,

respectively, which clearly demonstrated that a majority of the populations were externalized from the lipid bilayer and stayed as solvent exposed (Fig. 4).

These observations are analogous with the mutational results observed in the previous section (Figs. 2 and 3) where substitutions in these residue positions (S16, A17) significantly affected the TMD1 externalization process. However, externalization of TMD1, while nitroxide spin labels were introduced in those positions, is more likely linked to the change in the intramolecular or intermolecular interactions with TMD2 rather than changes in TMD1 hydrophobicity and implies the significance of those residue positions for the native structural conformations.

To visualize the relative effect of each individual mutation on the relative population of  $S^{21}68_{IRS}$  TMD1, calculated depth parameters are summarized in Fig. 5.

Fig. 5 clearly indicates that the increased hydrophilicity at A17, G14, and A16 positions increased the propensity of S<sup>21</sup>68<sub>IRS</sub> TMD1 to externalize. Hence, more populations adapt the active conformation. However, the increased hydrophobicity at A17 and A16 positions prevented S<sup>21</sup>68<sub>IRS</sub> TMD1 externalization (Fig. 5). Additionally, the placement of the R1 spin label at A17 and S16 also caused the externalization of  $S^{21}68_{IRS}$  TMD1. These results suggest that some pinholin  $S^{21}$  residue positions such as G14, S16 and A17 have a significant effect on the protein's structural topology as the mutation to those positions induces significant structural perturbation. It is important to mention here that TMD1 has a putative glycine zipper (G10xxxG14xxxG18), which may have a significant role on the structural conformation of pinholin S<sup>21</sup>. In the inactive conformation of S<sup>21</sup>, TMD1 remains inside of the lipid bilayer and interacts with the TMD2 of the same monomer or the adjacent molecules of the dimer [24]. Hence, this glycine zipper region plays a crucial role for the molecular packing and hydrophobic interaction. Certain changes in this region may cause structural perturbations and alter the rate of activation of pinholin by altering the TMD1 externalization process. Hence, these types of residues should be avoided during the SDSL to study the native structural topology of a similar system.

# 3.2. Pinholin conformational changes observed with DEER distance measurements

The CW-EPR power saturation data represent whether a majority of the population is located inside or outside of the lipid bilayer and are more applicable to studying systems with a single conformation. DEER

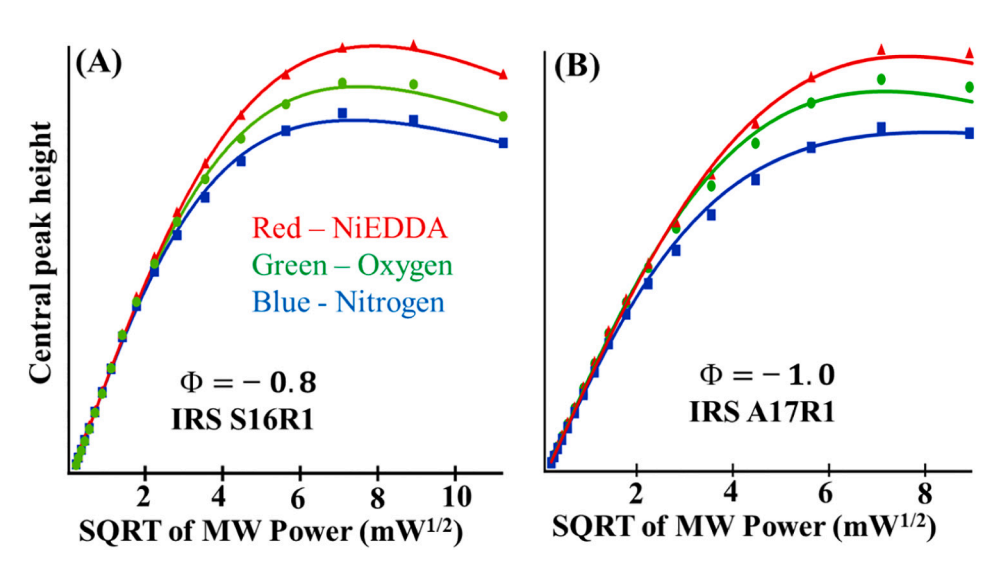
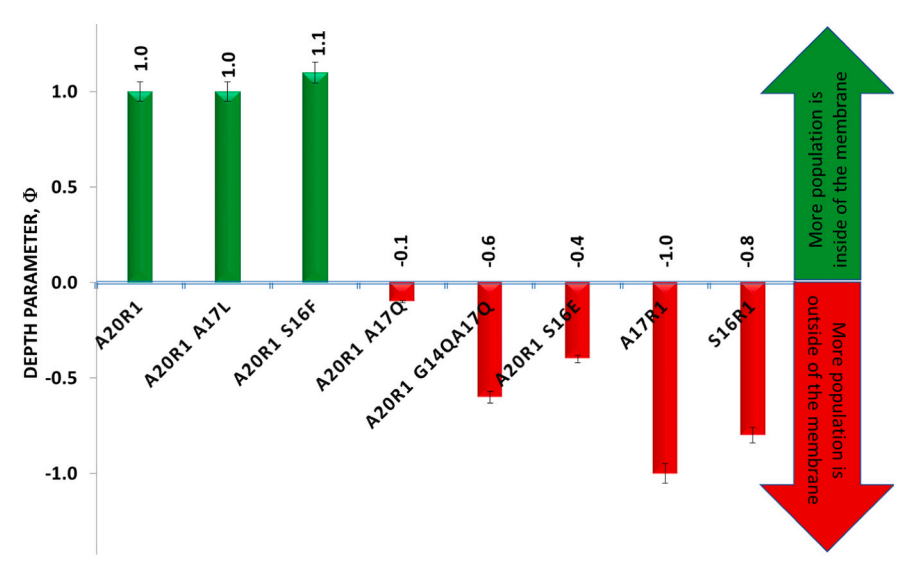


Fig. 4. Effect of MTSL on the externalization of  $S^{21}68_{IRS}$  TMD1. CW-EPR power saturation data collected for variants (A) IRS S16R1 and (B) IRS A17R1. Respective depth parameters are shown with the uncertainty of  $\pm 5\%$ .



**Fig. 5.** Comparison of the depth parameter for different  $S^{21}68_{IRS}$  mutants with respect to the IRS\_A20R1. The red columns indicate a negative depth parameter where a majority of the spin label was outside of the lipid bilayer. The green columns indicate a positive depth parameter where a majority of the spin label was inside of the lipid bilayer. Respective depth parameters are shown on each bar with the error bar of  $\pm 5\%$ . (For interpretation of the references to color in this figure legend, the reader is referred to the web version of this article.)

spectroscopy is a powerful biophysical technique that can provide direct evidence of the conformational changes of biomolecules and relative population of multiple conformations by monitoring the spin label distance distribution [42,48–53]. To further validate EPR power saturation results and directly provide the evidence of the effect of mutations on pinholin conformational change, the DEER spectroscopic technique was employed. For DEER spectroscopic measurements, two spin labels were attached at S8 and L53 in S2168<sub>IRS</sub> and this construct was denoted as IRS\_S8R1/L53R1. These positions were selected as an anchoring point since they are located at the N-terminus side of TMD1 and the C-terminus side of TMD2, respectively. These two residues were also found in close proximity in the inactive conformation of antipinholin  $S^{21}68_{IRS}$ with a reported average distance of (26  $\pm$  4) Å [29]. Additionally, no significant functional and structural perturbations have been reported for mutations at these positions [24,29]. This construct will demonstrate a distinction of distance distribution between the inactive conformation of pinholin S<sup>21</sup>68<sub>IRS</sub> against any structural perturbation induced by the mutation. Three more constructs were designed with single, double, and triple mutations based on our CW-EPR power saturation results (see previous section) and those reported by Pang et al. (2010) [24]. These constructs were denoted as IRS\_S8R1/L53R1\_A17Q, IRS\_S8R1/ L53R1\_A17Q/G21Q, and IRS\_S8R1/L53R1\_G14Q/A17Q/G21Q with the spin labels at the S8 and L53 positions. The DEER distance distributions obtained from DEER measurements were then compared with that of the IRS\_S8R1/L53R1 (Fig. 6).

From inspection of the DEER distance distribution data (Fig. 6B), it is obvious that all mutant constructs showed a shorter distance peak centered around 26 Å similar to that of IRS\_S8R1/L53R1, and another distance population at around 49 Å (Fig. 6B). This longer distance population was not prominent for the single mutant IRS\_S8R1/ L53R1\_A17Q (Fig. 6B). However, the longer distance population was increased in the double mutation variant (IRS S8R1/L53R1 A17Q/ G21Q) and was further pronounced for the triple mutation variant (IRS S8R1\_L53R1\_G14Q/A17Q/G21Q) (Fig. 6B). These data clearly demonstrated that increased hydrophilicity at those residue positions enhanced the externalization of TMD1 and that a subpopulation was moving apart from TMD2, whereas others remained in close proximity as in the inactive conformation. The propensity of externalization increased with increased hydrophilicity and a cumulative effect was seen with the incorporation of additional mutations. This mutational effect is consistent with the power saturation data that indicated a higher number of populations of TMD1 were externalized when the hydrophilicity of TMD1 was increased. These results are also consistent with the mutational results reported by Pang et al. (2010) where G14Q, A17Q, and

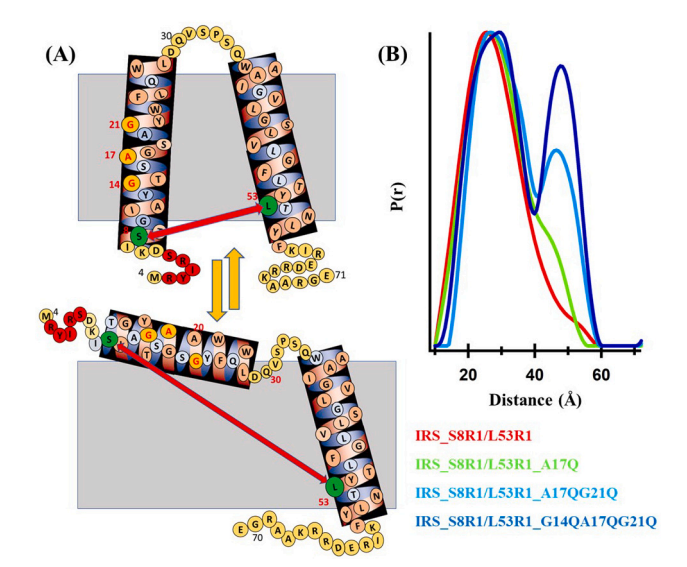


**Fig. 6.** Effect of mutations on DEER distance distributions of IRS\_S8R1/L53R1 with or without additional mutations. (A) Inactive and active conformation of  $S^{21}68_{IRS}$ . Spin label positions are shown in green and mutation points are shown as a red letter in the orange circles. (B) Distance probability distributions are color-coded as the same color of the construct name. The highest distances distributions are normalized to one. (For interpretation of the references to color in this figure legend, the reader is referred to the web version of this article.)

G21Q mutations caused activation of the dominant antipinholin  $S^{21}68_{IRS},$  although those mutants took additional time to trigger lysis [24]. DEER data clearly indicate that the activation of antipinholin  $S^{21}68_{IRS}$  is associated with the enhancement of the externalization of TMD1 due to the increased hydrophobicity of TMD1.

In addition to the mutational effects caused by natural amino acids, structural perturbations were also observed due to the presence of spin labels themselves, as was observed for CW-EPR power saturation experiments. A previous study showed that parallel distances between TMD1 and TMD2 of inactive pinholin were  $\sim$ 23–26 Å [29]. However, several dual-spin labeled antipinholin constructs, IRS\_S16R1/G48R1, IRS\_S16R1/V46R1, and IRS\_A20R1/L45R1 independently showed a longer distance distribution around 49 Å, 48 Å, and 45 Å, respectively with the uncertainty of  $\pm$ 4 Å (Fig. 7). These distances match more

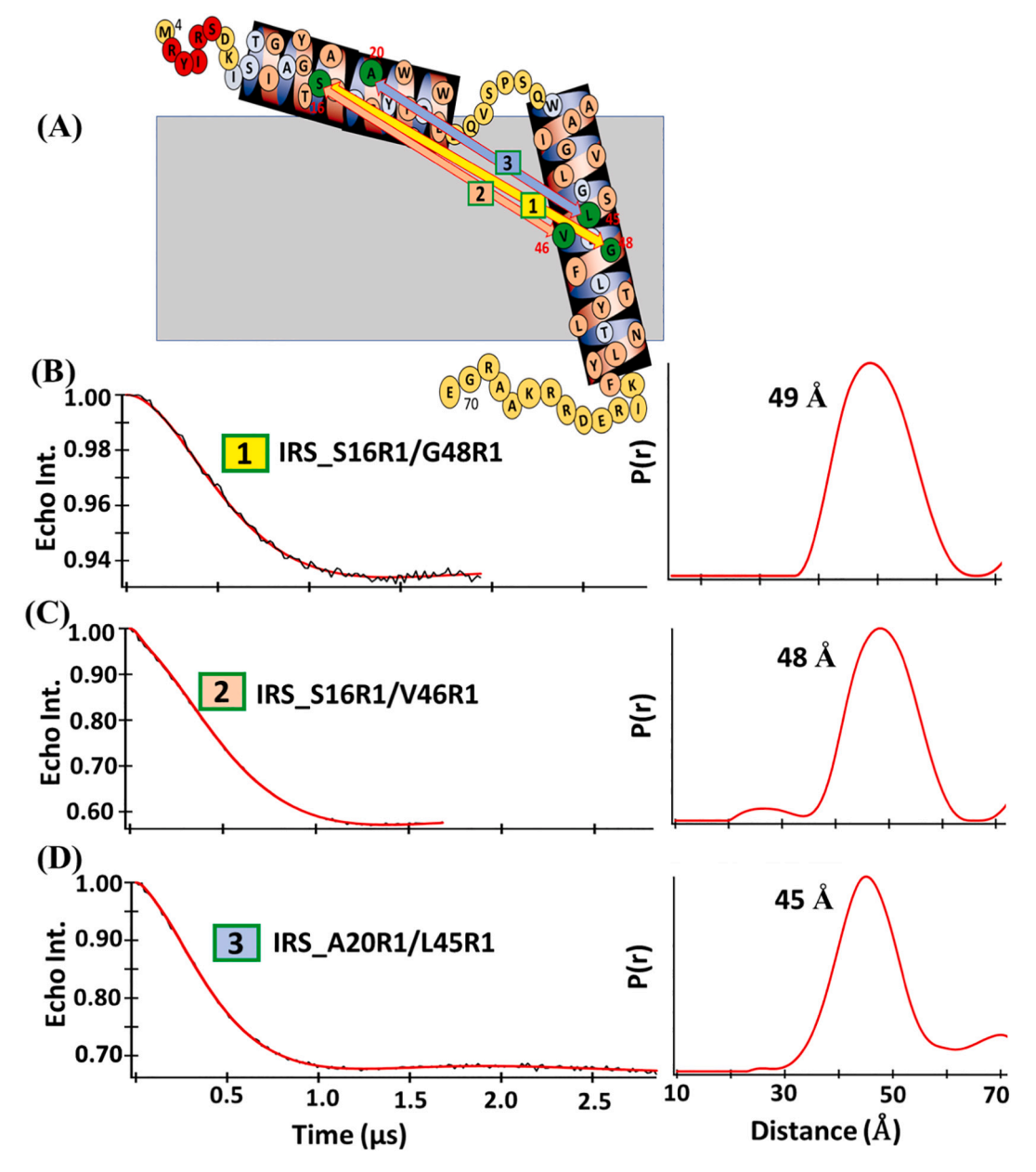


Fig. 7. Conformation change of antipinholin  $S^{21}68_{IRS}$  while spin labels were introduced at certain residue positions. Pair wise spin label positions and probable distances are shown with arrows for active conformation of  $S^{21}$  (A). DEER time domain spectrum and corresponding distance distribution for IRS\_S16R1/G48R1 (B), IRS\_S16R1/V46R1 (C), IRS\_A20R1/L45R1 (D) with the uncertainty of  $\pm 4$  Å. (The First spectrum was collected with 10 W amplifier).

closely with the active conformation of pinholin  $S^{21}$  instead of the inactive conformation which implies that the spin label at those residue positions caused a structural perturbation and externalized the TMD1 of antipinholin from the lipid bilayer.

In these DEER samples, one or both residue positions where spin labels were incorporated could induce structural perturbations due to the changes in intra and inter molecular interactions. In the earlier section (Fig. 4), CW-EPR power saturation data demonstrated that IRS\_S16R1 had an influence on the externalization of TMD1, which could be one of the reasons for the active conformation of IRS\_S16R1/G48R1, and IRS\_S16R1/V46R1 (Fig. 7). In addition, G40xxxS44xxxG48 is the glycine zipper present in TMD2 and has a significant effect on the structural conformation and oligomerization of S<sup>21</sup> pinholin [24]. Any residue in this region (e.g. L45, V46, G48) may contribute to the structural perturbation in addition to the mutational effects from TMD1. The mutational effects observed in the current study were based on the incorporation of the pinholin protein into the DMPC lipid bilayer. These

mutational effects may vary in different lipid bilayers. Further studies with different types of lipid bilayers are needed to generalize the mutational effect in the membrane environment. Similarly, a more detailed study is needed to explore further mutational points and the underlying mechanisms for the structural perturbations caused by those residue mutations.

## 4. Conclusion

This is the first EPR spectroscopic study which showed direct evidence of structural perturbation of pinholin  $S^{21}$  by positional mutations. This work also correlated these mutations with conformational changes and functionality of pinholin  $S^{21}$ . The CW-EPR power saturation and DEER data clearly demonstrated that the relative hydrophobicity and interaction of different residues impact the observed conformational changes that have been directly linked to the pinholin  $S^{21}$  activation and triggering time. This study judiciously utilized CW-EPR power

saturation and DEER spectroscopy to probe the effects of several amino acid residue mutations on antipinholin  $S^{21}68_{IRS}$  TMD1 externalization. This approach will pave the way for the application of additional biophysical techniques for mutational studies in several other biologically significant systems, especially those in which point mutations are likely related to functional/structural changes.

#### Declaration of competing interest

The authors declare the following financial interests/personal relationships which may be considered as potential competing interests:

Gary Lorigan reports financial support was provided by NIGMS. Gary Lorigan reports financial support was provided by NSF.

#### Acknowledgments

We are grateful to the members of the Ry Young group at Texas A&M University for their experimental suggestions. This work was generously supported by NSF CHE-1807131 grant, NSF (MRI-1725502) grant, NIGMS/NIH Maximizing Investigator's Research Award (MIRA) R35 GM126935 award the Ohio Board of Regents, and Miami University. Gary A. Lorigan would also like to acknowledge support from the John W. Steube Professorship. Indra D. Sahu would also like to acknowledge support from the NSF MCB-2040917 award.

#### Appendix A. Supplementary data

Supplemental information includes figures for raw spectra of CW-EPR power saturation and DEER experiments, DEER data validation, peptide vs lipid ratio optimization for DEER experiments and one table for calculated  $P_{1/2}$  and  $\Phi$  values. Supplementary data to this article can be found online at https://doi.org/10.1016/j.bbamem.2021.183771.

#### References

- [1] T. Park, D.K. Struck, J.F. Deaton, R. Young, Topological dynamics of holins in programmed bacterial lysis, Proc. Natl. Acad. Sci. U. S. A. 103 (52) (2006) 10713 10718
- [2] M.R.J. Clokie, A.D. Millard, A.V. Letarov, S. Heaphy, Phages in nature, Bacteriophage 1 (2011) 31–45.
- [3] I.N. Wang, D.L. Smith, R. Young, Holins: the protein clocks of bacteriophage infections, Annu. Rev. Microbiol. 54 (2000) 799–825.
- [4] R. Young, Bacteriophage holins: deadly diversity, J. Mol. Microbiol. Biotechnol. 4 (1) (2002) 21–36.
- [5] R. Young, Phage lysis: three steps, three choices, one outcome, J. Microbiol. 52 (3) (2014) 243–258.
- [6] J. Berry, M. Rajaure, T. Pang, R. Young, The spanin complex is essential for lambda lysis, J. Bacteriol. 194 (20) (2012) 5667–5674.
- [7] J. Berry, E.J. Summer, D.K. Struck, R. Young, The final step in the phage infection cycle: the rz and Rz1 lysis proteins link the inner and outer membranes, Mol. Microbiol. 70 (2) (2008) 341–351.
- [8] A. Graschopf, U. Blasi, Functional assembly of the lambda S holin requires periplasmic localization of its N-terminus, Arch. Microbiol. 172 (1) (1999) 31–39.
- [9] N. Zhang, R. Young, Complementation and characterization of the nested rz and Rz1 reading frames in the genome of bacteriophage lambda, Mol. Gen. Genet. 262 (4–5) (1999) 659–667.
- [10] T. Pang, C.G. Savva, K.G. Fleming, D.K. Struck, R. Young, Structure of the lethal phage pinhole, Proc. Natl. Acad. Sci. U. S. A. 106 (45) (2009) 18966–18971.
- [11] I.N. Wang, J. Deaton, R. Young, Sizing the holin lesion with an endolysin-beta-galactosidase fusion, J. Bacteriol. 185 (3) (2003) 779–787.
- [12] J. Cahill, R. Young, Phage lysis: multiple genes for multiple barriers, Adv. Virus Res. 103 (2019) 33–70.
- [13] C.Y. Chang, K. Nam, R.Y. Young, S-gene expression and the timing of lysis by bacteriophage-lambda, J. Bacteriol. 177 (11) (1995) 3283–3294.
- [14] R. Young, I.N. Wang, in: Phage lysis. The bacteriophages, 2nd ed., Oxford Univ Press, Oxford, 2006, pp. 104–126.
- [15] R. Young, Phage lysis: do we have the hole story yet? Curr. Opin. Microbiol. 16 (6) (2013) 790–797.
- [16] R.Y. Young, Bacteriophage lysis mechanism and regulation, Microbiol. Rev. 56 (3) (1992) 430–481.
- [17] U. Blasi, R. Young, Two beginnings for a single purpose: the dual-start holins in the regulation of phage lysis, Mol. Microbiol. 21 (4) (1996) 675–682.
- [18] C.G. Savva, J.S. Dewey, J. Deaton, R.L. White, D.K. Struck, A. Holzenburg, R. Young, The holin of bacteriophage lambda forms rings with large diameter, Mol. Microbiol. 69 (4) (2008) 784–793.

- [19] C.G. Savva, J.S. Dewey, S.H. Moussa, K.H. To, A. Holzenburg, R. Young, Stable micron-scale holes are a general feature of canonical holins, Mol. Microbiol. 91 (1) (2014) 57–65.
- [20] K.H. To, R. Young, Probing the structure of the S105 hole, J. Bacteriol. 196 (21) (2014) 3683–3689.
- [21] R. White, S. Chiba, T. Pang, J.S. Dewey, C.G. Savva, A. Holzenburg, K. Pogliano, R. Young, Holin triggering in real time, Proc. Natl. Acad. Sci. U. S. A. 108 (2) (2011) 798–803.
- [22] T. Park, D.K. Struck, C.A. Dankenbring, R. Young, The pinholin of lambdoid phage 21: control of lysis by membrane depolarization, J. Bacteriol. 189 (24) (2007) 9135–9139.
- [23] T. Pang, T. Park, R. Young, Mapping the pinhole formation pathway of S21, Mol. Microbiol. 78 (3) (2010) 710–719.
- [24] T. Pang, T. Park, R. Young, Mutational analysis of the S21 pinholin, Mol. Microbiol. 76 (1) (2010) 68–77.
- [25] T. Ahammad, D.L. Drew, I.D. Sahu, R.A. Serafin, K.R. Clowes, G.A. Lorigan, Continuous wave electron paramagnetic resonance spectroscopy reveals the structural topology and dynamic properties of active pinholin S(21)68 in a lipid bilayer, J. Phys. Chem. B 123 (38) (2019) 8048–8056.
- [26] D.L. Drew Jr., T. Ahammad, R.A. Serafin, B.J. Butcher, K.R. Clowes, Z. Drake, I. D. Sahu, R.M. McCarrick, G.A. Lorigan, Solid phase synthesis and spectroscopic characterization of the active and inactive forms of bacteriophage S21 pinholin protein, Anal. Biochem. 567 (2018) 14–20.
- [27] D.L. Drew Jr., B. Butcher, I.D. Sahu, T. Ahammad, G. Dixit, G.A. Lorigan, Active S2168 and inactive S21IRS pinholin interact differently with the lipid bilayer: A 31P and 2H solid state NMR study, Biochim. Biophys. Acta Biomembr. 183257–183257 (2020).
- [28] T. Pang, T.C. Fleming, K. Pogliano, R. Young, Visualization of pinholin lesions in vivo, Proc. Natl. Acad. Sci. U. S. A. 110 (22) (2013) E2054–E2063.
- [29] T. Ahammad, D.L. Drew Jr., I.D. Sahu, R.H. Khan, B.J. Butcher, R.A. Serafin, A. P. Galende, R.M. McCarrick, G.A. Lorigan, Conformational differences are observed for the active and inactive forms of pinholin S21 using DEER spectroscopy, J. Phys. Chem. B 124 (50) (2020) 11396–11405.
- [30] T. Ahammad, D.L. Drew, R.H. Khan, I.D. Sahu, E. Faul, T. Li, G.A. Lorigan, Structural dynamics and topology of the inactive form of S21 holin in a lipid bilayer using continuous-wave electron paramagnetic resonance spectroscopy, J. Phys. Chem. B 124 (26) (2020) 5370–5379.
- [31] L. Bottorf, I.D. Sahu, R.M. McCarrick, G.A. Lorigan, Utilization of C-13-labeled amino acids to probe the alpha-helical local secondary structure of a membrane peptide using electron spin echo envelope modulation (ESEEM) spectroscopy, Biochim. Biophys. Acta Biomembr. 1860 (7) (2018) 1447–1451.
- [32] D.J. Mayo, I.D. Sahu, G.A. Lorigan, Assessing topology and surface orientation of an antimicrobial peptide magainin 2 using mechanically aligned bilayers and electron paramagnetic resonance spectroscopy, Chem. Phys. Lipids 213 (2018) 124–130.
- [33] D. Needham, T.J. McIntosh, E. Evans, Thermomechanical and transition properties of dimyristoylphosphatidylcholine cholesterol bilayers, Biochemistry 27 (13) (1988) 4668–4673.
- [34] D. Marsh, Thermodynamics of phospholipid self-assembly, Biophys. J. 102 (5) (2012) 1079–1087.
- [35] L. Yu, W. Wang, S.L. Ling, S.L. Liu, L. Xiao, Y.L. Xin, C.H. Lai, Y. Xiong, L.H. Zhang, C.L. Tian, CW-EPR studies revealed different motional properties and oligomeric states of the integrin beta(1a) transmembrane domain in detergent micelles or liposomes, Sci. Rep. 5 (7848) (2015) 1–11.
- [36] W.L. Hubbell, C. Altenbach, Investigation of structure and dynamics in membraneproteins using site-directed spin-labeling, Curr. Opin. Struct. Biol. 4 (4) (1994) 566–573.
- [37] C. Altenbach, T. Marti, H.G. Khorana, W.L. Hubbell, Transmembrane protein structure: spin labeling of bacteriorhodopsin mutants, Science 248 (4959) (1990) 1088–1092.
- [38] C.A. Popp, J.S. Hyde, Effects of oxygen on electron-paramagnetic-res of nitroxide spin-label probes of model membranes, J. Magn. Reson. 43 (2) (1981) 249–258.
- [39] C.S. Klug, W.Y. Su, J.B. Feix, Mapping of the residues involved in a proposed betastrand located in the ferric enterobactin receptor FepA using site-directed spinlabeling, Biochemistry 36 (42) (1997) 13027–13033.
- [40] K.J. Oh, C. Altenbach, R.J. Collier, W.L. Hubbell, Site-directed spin labeling of proteins. applications to diphtheria toxin, Methods Mol. Biol. 145 (2000) 147–169.
- [41] C. Altenbach, D.A. Greenhalgh, H.G. Khorana, W.L. Hubbell, A collision gradient method to determine the immersion depth of nitroxides in lipid bilayers: application to spin-labeled mutants of bacteriorhodopsin, Proc. Natl. Acad. Sci. U. S. A. 91 (5) (1994) 1667–1671.
- [42] G. Jeschke, DEER distance measurements on proteins, Annu. Rev. Phys. Chem. 63 (63) (2012) 419–446.
- [43] M. Pannier, S. Veit, A. Godt, G. Jeschke, H.W. Spiess, Dead-time free measurement of dipole-dipole interactions between electron spins, J. Magn. Reson. 142 (2) (2000) 331–340.
- [44] G. Jeschke, V. Chechik, P. Ionita, A. Godt, H. Zimmermann, J. Banham, C. R. Timmel, D. Hilger, H. Jung, DeerAnalysis2006 - a comprehensive software package for analyzing pulsed ELDOR data, Appl. Magn. Reson. 30 (3–4) (2006) 473–498.
- [45] Y.W. Chiang, P.P. Borbat, J.H. Freed, The determination of pair distance distributions by pulsed ESR using tikhonov regularization, J. Magn. Reson. 172 (2) (2005) 279–295.
- [46] E. Bordignon, Site-directed spin labeling of membrane proteins, EPR Spectrosc. Appl. Chem. Biol. 321 (2012) 121–157.

- [47] I.D. Sahu, G.A. Lorigan, Site-directed spin labeling EPR for studying membrane proteins, Biomed. Res. Int. 3248289 (2018).
- [48] I.D. Sahu, G.A. Lorigan, Biophysical EPR studies applied to membrane proteins, J. Phys. Chem. Biophys. 5 (2015) 188.
- [49] G. Jeschke, Y. Polyhach, Distance measurements on spin-labelled biomacromolecules by pulsed electron paramagnetic resonance, Phys. Chem. Chem. Phys. 9 (16) (2007) 1895–1910.
- [50] P.P. Borbat, H.S. McHaourab, J.H. Freed, Protein structure determination using long-distance constraints from double-quantum coherence ESR: study of T4 lysozyme, J. Am. Chem. Soc. 124 (19) (2002) 5304–5314.
- [51] E.F. Vincent, I.D. Sahu, A.J. Costa-Filho, E.M. Chilli, G.A. Lorigan, Conformational changes of the HsDHODH N-terminal microdomain via DEER spectroscopy, J. Phys. Chem. B 119 (2015) 8693–8697.
- [52] I.D. Sahu, R.M. McCarrick, K.R. Troxel, R.F. Zhang, H.J. Smith, M.M. Dunagan, M. S. Swartz, P.V. Rajan, B.M. Kroncke, C.R. Sanders, et al., DEER EPR measurements for membrane protein structures via bifunctional spin labels and lipodisq nanoparticles, Biochemistry 52 (38) (2013) 6627–6632.
- [53] I.D. Sahu, R.M. McCarrick, G.A. Lorigan, Use of electron paramagnetic resonance to solve biochemical problems, Biochemistry 52 (35) (2013) 5967–5984.